Chapter 3. Studying the time-evolution of charged droplets generated by electrospray ionization in an ion mobility cell. The ping-pong experiment revisited

Portions adapted from Grimm, Ronald L.; Beauchamp, J. L. *Anal. Chem*. **2002**, *74*, 6291.

3.1. Introduction

Rather than use an electrodynamic balance to trap and hold droplets where the electric forces balance the force of gravity ($qE = mg$), the Beauchamp group employs an ion mobility spectrometer (IMS). In our IMS, $qE \neq mg$ and droplets are dragged through a linear electric field while being characterized according to size, equilibrium velocity, and net charge using a phase Doppler anemometer (PDA). This chapter reviews the theoretical and practical aspects of the experimental apparatus employed for the fundamental studies of droplet evaporation and discharge dynamics discussed in Chapters 4 and 5.

In this chapter, section 3.2 discusses the advantages and disadvantages of mobility studies. Section 3.3 reviews the instrumentation for these studies. Sections 3.4 and 3.5 introduce the equations of motion for a charged droplet and apply these equations of motion to a model for droplet behavior in the mobility cell. Section 3.5 presents the results from the model for droplets of varying size and charge as well as a discussion of the implication for mobility studies of evaporation and discharge dynamics.

3.2. The benefits of mobility measurements of charged droplets

Lord Rayleigh developed the critical theories of charged droplets, balancing the forces of surface tension and charge repulsion to determine charged droplet stability. His work suggests that, in a droplet of radius r and surface tension σ in a medium of electric permittivity ε, charge repulsion will overcome surface tension at a charge q_R given by equation (3.1). When this condition is met, Rayleigh predicts that droplets undergo a disruptive event in which "the liquid is thrown out in fine jets, whose fineness, however, has a limit". Although this suggests a mechanism for the discharge event, his model lacks a quantitative description of the charge loss and specific relationships between the parent and the progeny drop or droplets.[1]

$$q_R = 8\pi\varepsilon^{1/2}\sigma^{1/2}r^{3/2} \tag{3.1}$$

Many researchers have studied the dynamics of the evaporation, jetting, and progeny droplet formation associated with this event, termed Rayleigh discharge. As Table 2.1 notes, the majority of evaporation and Rayleigh discharge studies have been performed on low vapor pressure solvent droplets suspended in an electrodynamic balance (EDB). These studies generally conclude that charge loss is proportional to droplet surface tension, and the droplet undergoes discharge between 70 and 120% of its predicted Rayleigh limit. Additionally, the studies show that discharge events generally remove 10-40% of the parent droplet charge and only 1-5% of the parent droplet mass. Unfortunately, not all of the results support this conclusion. Indeed, even experiments performed within the past five years have generated vastly diverging results. Feng et al. note the loss of 80% of the net charge in the Rayleigh discharge events of methanol (σ = 0.022 N m^{-1}) droplets in an electrodynamic balance,[2] whereas Duft and co-workers

observe loss of 25 to 33% the net charge on ethylene glycol (σ = 0.048 N m^{-1}) droplets.[3,4] Such results suggest that different techniques are needed to compliment the existing picture of Rayleigh discharge phenomena.

In our laboratory, Smith and coworkers demonstrate that ion mobility spectrometry is an effective tool for Rayleigh discharge studies of higher vapor pressure solvents that are otherwise difficult to analyze in an EDB.[5,6] In the mobility cell, droplets are subjected to a linear, uniform ~50 V cm^{-1} electric field directed parallel or antiparallel to the force of gravity. Such field strengths produce negligible distortions to the droplet. Additionally, there are no fields providing radial trapping as exist in the electrodynamic balance experiments that might affect the droplet behavior.

3.3. Instrumentation

Figure 3.1 presents a schematic of the experimental apparatus. The instrument consists of three parts: the electrospray source that generates charged droplets in the 10-100 μm size range, the mobility cell (often referred to as a drift cell or the drift region), and a phase Doppler anemometer (PDA) that characterizes droplet size, velocity and charge. Smith presents an excellent review of the hardware, experimental procedures and data analysis,[5] and the instrument has been described several times in the literature.[6,7] This section summarizes the critical aspects of the hardware and provides context for the Rayleigh discharge studies presented in Chapters 4 and 5.

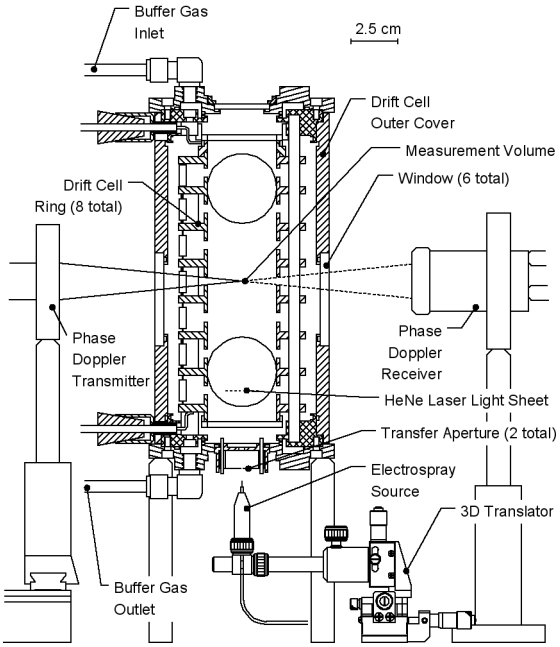

Figure 3.1. Schematic representation of the apparatus employed for droplet evaporation and discharge studies. Droplets are generated by the electrospray source and directed through two apertures into the drift region of the ion mobility cell. Droplet "ping-pong" commences when a droplet passes through the measurement volume of the phase Doppler anemometer. Adapted from Grimm and Beauchamp.[7]

3.3.1. Electrospray ionization source

Droplets are produced at the electrospray ionization source and directed upward through the ion mobility spectrometer (IMS) drift cell for analysis. A polished hypodermic stainless steel needle (R-HTX-35, 64 μm i.d., 150 μm o.d., Small Parts, Inc.) mounted on a three-dimensional stage sprays upward through two sequential apertures on the bottom of the drift cell. The first aperture is 500 μm in diameter and biased at +100 V. One centimeter above the first, the second aperture is 1.5 mm in diameter and maintained at earth ground. To generate positively charged droplets between 10 and 60 μm in diameter, the electrospray needle is biased between +800 and +1200 V, and the distance between the hypodermic needle tip and the first aperture is adjusted between 0.5 and 5 mm. Our experimental arrangement selects droplets close to the axis of the spray. Solvents are used without further purification. In all cases, solution flow rates are 0.2-0.5 μL min^{-1} and dry nitrogen gas flows downward through the cell at 0.3 L min^{-1} or 0.6 cm s^{-1}.

3.3.2. Ion mobility cell and the ping-pong technique

Eight vertically stacked, resistively coupled, stainless steel rings define a 20 cm-long, 4 cm-inner diameter drift region within the IMS. Dry nitrogen gas at ambient temperature (293 K) flows downward through the drift cell to ensure the droplets are evaporating in an environment free from solvent vapor. In the center of the cell, 10 cm above the electrospray source, two intersecting HeNe laser beams form the measurement volume, roughly 150 μm in diameter, of the phase Doppler anemometer (PDA). The phase Doppler anemometer acquires the velocity and diameter of the droplet. These

values yield the net droplet charge through a force-balance equation of motion discussed later in this chapter.

A 50.6 V cm^{-1} electric field initially directs positively charged droplets upward through the cell. Droplets initially travel at 50 cm s^{-1} taking ~200 ms to reach the PDA measurement volume discussed in Section 3.3.3. Data used to determine droplet size and velocity are acquired by the PDA and recorded using a digital oscilloscope when a droplet drifts upwards through the measurement volume. The oscilloscope triggers two high-voltage MOSFET switches (MTP1N100E, Motorola) that reverse the cell voltages causing the droplet to travel downward towards the measurement volume. Subsequent PDA detection and field switching repeats at roughly 100 Hz and the droplet undergoes a ping-pong motion through the measurement volume until it is no longer detected, either because of evaporation to an undetectable size (~1 μm) or from radially drifting beyond the measurement volume. The latter is the principle reason for terminating acquisition, as no radial trapping force exists in the cell. Droplet ping-pong and PDA analysis records a history of the diameter, velocity, and charge sampled roughly every 10 ms. Percent Rayleigh limit is determined by the ratio of the charge to q_R, calculated by equation (3.1).

3.3.3. Phase Doppler anemometer

The phase Doppler assembly consists of a transmitter and receiver shown in Figure 3.2. In the transmitter, a Helium-Neon (HeNe) laser generates $\lambda = 632.8$ nm linearly polarized light for the transmitter. The beam passes through a two-lens beam expander followed by a prism that separates the original beam into two parallel beams

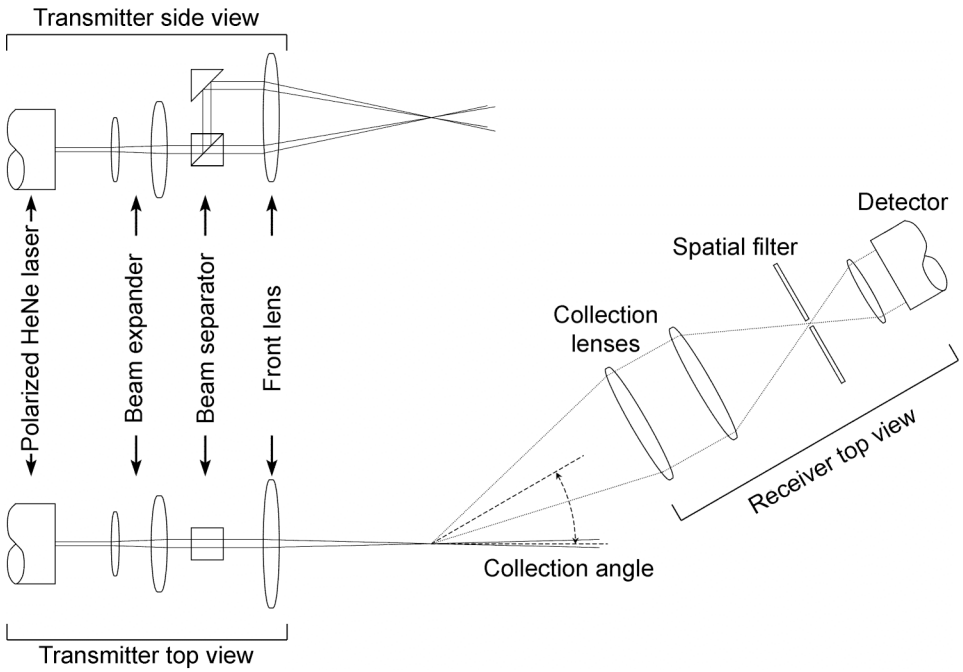

Figure 3.2. Schematic of the phase Doppler anemometer arrangement. In the transmitter array, light generated by a helium neon laser passes through a two-lens beam expander and is split with a beam separator into two parallel beams. The front lens directs the beams together where the interference fringes define the measurement volume. Scattered light is collected by the receiver array where collection lenses direct light through a spatial filter onto a two-element photodiode array.

with a well-defined spacing, *s*. A focusing lens with focal length *F* directs the beams to a measurement volume consisting of a series of constructive and destructive interference fringes stacked parallel to the laser propagation plane. When $s << F$, the fringe spacing, δ, is approximated by eq (3.2).

$$\delta \approx \frac{\lambda F}{s} \tag{3.2}$$

The beam waist diameter, D_w, of the laser beams passing through the focusing lens determines the size of the measurement volume, shown in eq (3.3).

$$D_w = \frac{4\lambda F}{\pi D_{beam}} \tag{3.3}$$

In eq (3.3), D_{beam} represents the diameter of the laser beams prior to passing through the focusing lens. In this experiment D_{beam} is twice the diameter of the beam generated by the laser as a result of the 2*x* beam expander. The number of fringes in the measurement volume is approximately D_w / δ. For a typical configuration in which $s = 23$ mm and $F = 250$ mm, the fringe spacing is approximately 6.9 μm and the measurement volume waist diameter is ~200 μm, which provides approximately 29 usable fringes.

Droplets scatter light that is then detected by the PDA receiver assembly. This assembly consists of two collection lenses that direct the scattered light through a spatial filter and onto a detector consisting of two vertically stacked photodiode elements. The receiver assembly is mounted in the scattering plane and 30° off-axis of the laser propagation plane to maximize the Mie-scattered light while minimizing interference from the transmitter itself. As a droplet passes upwards into the measurement volume, the scattered light sweeps upwards past the collection lenses. The signal at the lower photodiode leads the upper photodiode with a phase shift well defined by the curvature of

the droplet. The PDA receiver detects velocity information because light scattered from each fringe arrives at the detectors temporally separated. Droplet velocity is computed from this time spacing and the fringe spacing defined in eq (3.2). Droplet size is computed from numerical solutions relating the phase shift of the detector signals to the curvature of the droplet.

3.4. Equations of motion of a droplet in the ion mobility cell

Size and velocity information from the phase Doppler anemometer may be inserted into a force balance equation to determine droplet charge. Deriving equations of motion of a droplet under the influence of multiple forces begins with a generalized force balance eq (3.4) where m_p is the particle mass, v is the velocity, t is time, and F_i is the contribution of the ith force.

$$m_p \frac{d}{dt} v = \sum_i F_i \tag{3.4}$$

In the case of a droplet with charge $q \neq 0$ under the influence of an electric field, gravity, and atmospheric drag, the force balance equation is represented by eq (3.5).

$$m_p \frac{d}{dt} v = F_{field} + F_{gravity} - F_{drag} \tag{3.5}$$

For consistency, motion upwards (against gravity) is defined as a positive velocity and motion downwards (with gravity) is defined as negative. When the electric field, E, is aligned antiparallel to gravity, $F_{field} = +qE$ resulting in upwards motion and $-qE$ when parallel to gravity resulting in downwards motion. The force of gravity is always downwards, thus $F_{gravity} = -m_p g$. Here g is the accelleration due to gravity, E is the electric field strength, and q is the net charge. Since atmospheric drag dampens droplet

motion F_{drag} always opposes the direction of velocity. Therefore, the sign of F_{drag} always opposes the sign of v. For the case of spherical droplets between 1 and 100 μm in diameter, the force of drag due to the atmosphere is given by equation (8.31) in Seinfield and Pandis[8] divided by the Cunningham slip correction factor, C_c, shown in eq

$$F_{drag} = \frac{\pi C_D \rho_{air} d_p^2 v^2}{8 C_c} \tag{3.6}$$

In (3.6), where C_D is the drag coefficient, ρ_{air} is the density of air, and d_p is the droplet diameter. Combining the terms, eq (3.7) expresses eq (3.5) with the appropriate force equations for droplets being directed upwards through the drift cell.

$$m_p \frac{d}{dt} v = qE - m_p g - \frac{\pi C_D \rho_{air} d_p^2 v^2}{8 C_c} \tag{3.7}$$

When the forces acting on the droplet are in equilibrium and there is no net acceleration, $dv / dt = 0$ and eq (3.7) simplifies to give the velocity of a droplet as a function of size and charge in eq (3.8) or the charge on the droplet as a function of size and velocity in eq (3.9).

$$v = \left[\frac{8 C_c}{\pi C_D \rho_{air} d_p^2} \left(qE - m_p g \right) \right]^{1/2} \tag{3.8}$$

$$q = \frac{\pi C_D \rho_{air} d_p^2 v^2 + 8 C_c m_p g}{8 C_c E} \tag{3.9}$$

Equations (3.8) and (3.9) apply to upwards drift in the cell. Equation (3.10) represents the charge when the electric field is reversed and droplets are directed downwards through the cell.

$$q = \frac{\pi C_D \rho_{air} d_p^2 v^2 - 8 C_c m_p g}{8 C_c E} \tag{3.10}$$

3.5. Modeling droplet behavior to determine droplet relaxation time

The assertion of equilibrium is critical to determining droplet charge from the phase Doppler data. For droplets under the influence of drag and gravity, Seinfeld and Pandis calculate the characteristic relaxation time, τ, given by equation (8.38) in their text and equation (3.11) below.[8] Tau represents the time to reach $1 - e^{-1}$ or 63% of the equilibrium velocity as a function of size and drag factors.

$$\tau = \frac{m_p C_c}{3\pi\mu_{air} d_p} \tag{3.11}$$

Figure 3.3 shows a plot of eq (3.11) for water and methanol droplets in the size range studied in the ping-pong experiment. The millisecond order of magnitude is close to the 10 ms sampling time indicating that the droplets might not have reached their equilibrium velocity before being sampled. Additionally, eq (3.11) represents the characteristic relaxation time of a droplet only under the force of gravity and atmospheric drag; the effect of an electric field is not considered. Modeling droplet behavior using equation (3.5) is necessary for a complete understanding of droplet behavior within the cell.

3.5.1. Modeling the droplet motion using Euler's Method

Because the previously discussed relaxation time does not consider the effect of an applied electric field, numerical methods can determine whether droplets passing through the measurement volume have reached their terminal velocity. To apply eq (3.5), Euler's method determines the velocity, *v*, and position, *z*, after *i* timesteps as a function

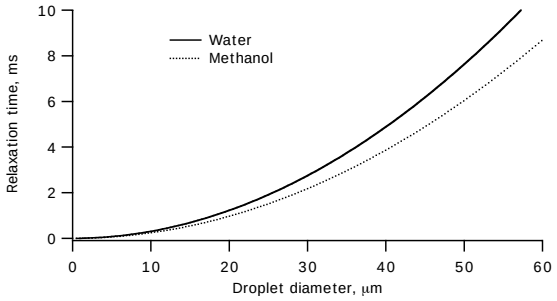

Figure 3.3. Characteristic relaxation time for a droplet under the influence of gravity and atmospheric drag. Both methanol and water droplets in the micron size regime reach their terminal velocity in milliseconds.

of time according to equations (3.12) and (3.13) respectively. The model is applied in Microsoft Excel and Igor Pro (WaveMetrics, Lake Oswego, Oregon).

$$v_{i+1} = v_i + \Delta t \frac{d}{dt} v_i \tag{3.12}$$

$$z_{i+1} = z_i + \Delta t v_i \tag{3.13}$$

In this model dv_i / dt is determined by (3.5). Initially the droplet starts out at the measurement volume defined as $z = 0$ with some initial positive, upward velocity v_0.

Rules for changing the sign of F_{drag} and F_{field} determine the ping-pong behavior of the droplet. The sign of F_{drag} is always opposite of the sign of v since the drag force always opposes droplet motion. Each time the droplet passes through $z = 0$, the electric field reverses. However, because of delays inherent in the electronics, there is always a lag between the droplet passing through the measurement volume and the field reversal. Thus the model field does not switch until a delay time t_d after a $z = 0$ event occurs corresponding to the droplet passing through the measurement volume.

This model determines droplet position and velocity for 50 ms using 25 μs timesteps. No significant difference is observed when using a fourth-order Runge-Kutta numerical method to calculate velocity and position rather than Euler's method.[9] This is attributed to the small, 25 μs timestep employed in the method.

3.5.2. Model results as a function of droplet size

Figure 3.4 presents the model results for 50 μm (frame A), 30 μm (frame B) and 10 μm (frame C) diameter water droplets at their Rayleigh limit of charge. In all cases

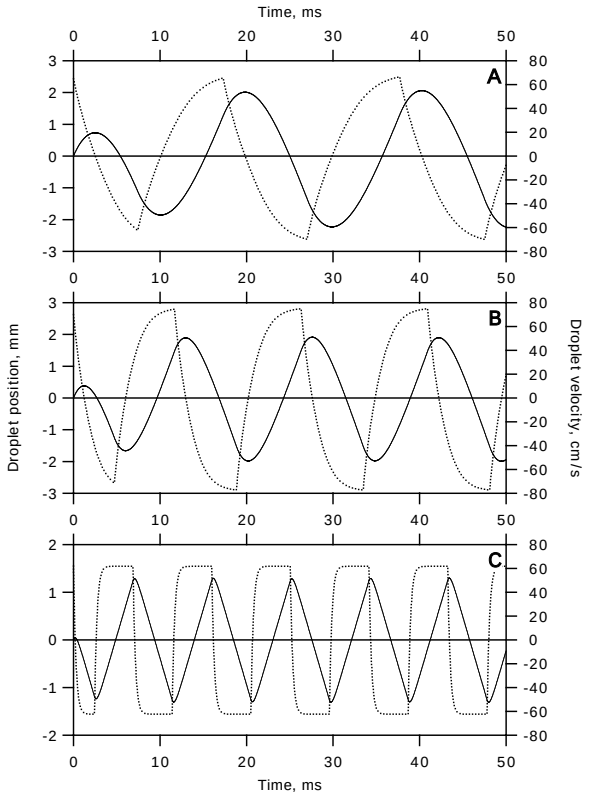

Figure 3.4. Position (solid) relative to the measurement volume and velocity (dotted) versus time for (A) 50 μm, (B) 30 μm, and (C) 10 μm diameter water droplets at their Rayleigh limit in our mobility cell. Because the velocity does not level off at each step, the 50 μm droplets are most likely not at equilibrium when characterized by the PDA. The 10 μm droplets are at equilibrium and the 30 μm droplets are close to equilibrium.

the applied electric field is 50 V cm^{-1} and t_d = 2 ms. The velocity plots (dotted curve) show that 50 μm droplets do not reach their equilibrium velocity before the field is reversed. The relaxation time for 50 μm droplets is estimated to be greater than 10 ms. The 30 μm droplets are closer to reaching their equilibrium velocity, but these too are not at equilibrium when they pass through the measurement volume. The relaxation time for 30 μm droplets is less than 10 ms. Conversely, the 10 μm droplets reach their equilibrium velocity within 2 ms of a field reversal. The results demonstrate that smaller droplets reach equilibrium much more rapidly than larger droplets. This is in agreement with Seinfeld and Pandis for droplets under the influence only of gravity.[8] Because the 50 μm droplets are not yet in equilibrium, eqs (3.9) and (3.10) would introduce significant error in the calculated charge since q is proportional to v^2. Conversely, 10 μm droplets do reach equilibrium and therefore are well modeled by eqs (3.9) and (3.10).

3.5.3. Model results as a function of droplet charge

Figure 3.5 presents the behavior of 50 μm water droplets at 100% (frame A), 50% (frame B), and 10% (frame C) of their Rayleigh limit of charge. The Rayleigh limit for a 50 μm water droplet is 1.57×10^7 elementary charges. In all cases, droplets do not reach their equilibrium velocities indicating that droplet charge is not as important a parameter as diameter. In all cases the droplet's motion is centered below $z = 0$ because the droplets travel downwards faster than they travel upwards as a result of $F_{gravity}$. However, the effect is not as pronounced until low charge values as seen in Figure 3.5C with 10% of the Rayleigh limit of charge. In this case qE is only twice as large as $m_p g$, whereas qE is twenty times larger than $m_p g$ for 50 μm water droplets at the Rayleigh limit (frame A).

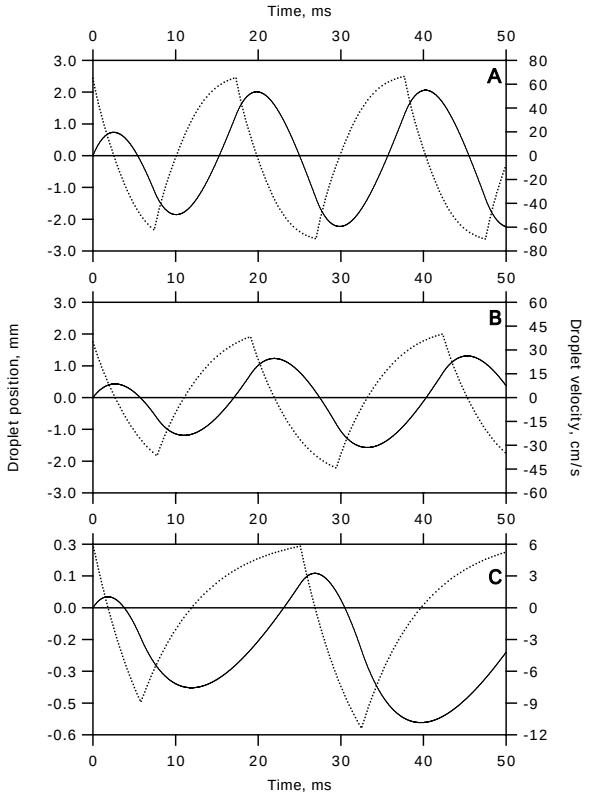

Figure 3.5. Position (solid) relative to the measurement volume and velocity (dotted) versus time for 50 μm diameter water droplets at (A) 100%, (B) 50%, and (C) 10% of their Rayleigh limit of charge. None of these droplets reach equilibrium before reaching the PDA.

3.6. Evaporation of micron-sized droplets within the IMS

For micron-size particles, droplets are significantly larger than the mean free path in air, 0.065 μm. In this continuum regime, evaporation is dominated by the rate at which vapor diffuses away from the droplet surface.[10] Following the notation and derivation similar to Hinds, eq (3.14) determines the evaporation rate for single-component droplets.[10]

$$\frac{d}{dt}d_{\mathrm{p}} = \frac{-4D_{ij}\left(T_{\mathrm{p}}\right)M}{R\rho_{\mathrm{p}}d_{\mathrm{p}}}\frac{p_{\mathrm{p}}\left(T_{\mathrm{p}}\right)}{T_{\mathrm{p}}} \tag{3.14}$$

In eq (3.14), solvent-specific parameters include $D_{ij}(T_{\mathrm{p}})$, the temperature-dependent diffusivity of solvent vapor i in gas j, solvent molar mass M, droplet density ρ_{p}, and equilibrium vapor pressure, $p_{\mathrm{p}}(T_{\mathrm{p}})$, at equilibrium surface temperature T_{p}, while R is the gas constant. This is simplified from a more rigorous model in which solvent vapor in the ambient gas inhibits evaporation. Experimentally, a constant flow of dry nitrogen gas through the apparatus flushes solvent vapor allowing for this simplification. Integrating the evaporation rate yields eq (3.15).

$$d_{\mathrm{p}}^2 = d_{\mathrm{o}}^2 + st \tag{3.15}$$

Equation (3.15) clusters the solvent-specific parameters into a single variable, s, given by eq (3.16).

$$s = -\frac{8D_{ij}(T_{\mathrm{p}})M}{R\rho_{\mathrm{p}}}\frac{p_{\mathrm{p}}(T_{\mathrm{p}})}{T_{\mathrm{p}}} \tag{3.16}$$

Spontaneous evaporation is endothermic, lowering the surface temperature to a size-independent equilibrium value, T_{p}, given by eq (3.17).

$$T_p = T_\infty - \frac{D_{ij}(T_p)\Delta H_{vap}(T_p)}{Rk_v(T_p)} \frac{p_p(T_p)}{T_p} \tag{3.17}$$

The surface temperature, T_p, is determined by the ambient gas temperature, T_∞, and thermodynamic values $\Delta H_{vap}(T_p)$ and k_v, the heat of vaporization and the thermal conductivity of the medium, respectively. Equation (3.17) must be iteratively solved for the equilibrium temperature because several parameters are temperature dependent. Heat of vaporization and vapor pressure data from Yaws[11] and diffusivity data from Vargaftik et al.[12] are inserted into eqs (3.15) through (3.17) for the evaporation of the three hydrocarbon solvents described in Chapter 4, as well as for methanol, acetonitrile, and water for comparison with previous studies.[6] The diffusivity for *p*-xylene was approximated by using the value for toluene. Table 3.1 lists the calculated solvent parameters, *s*, for the evaporation of acetonitrile, methanol, water, heptane, octane and *p*-xylene. As suggested by equations (3.15)-(3.17) and Table 3.1, *s* is a useful variable for quickly quantifying the evaporation rate of a particular solvent. Rapidly evaporating solvents have particularly large values of *s* while more slowly evaporating solvents have smaller values.

When ascertaining the timescales of the processes involved in the ping-pong experiment, it is also often useful to know the lifetime of a droplet. This is approximated by equation (3.15) when d_p is set to zero. Therefore, the lifetime of a particle is approximately $-d_o^2/s$. Using the values of *s* in Table 3.1, the lifetime of a 50 μm droplet ranges from 210 ms for *n*-heptane to up to 2 seconds for water.

	dielectric constant, ε	surface tension, γ (mN s^{-1})	evaporation temperature, T_p (K)	theoretical slope, s (μm^2 s^{-1})
Acetonitrile	36.64	28.66	270	-6500
Methanol	33.0	22.07	267	-4750
Water	74.6	71.99	278	-1250
n-Heptane	1.921	19.65	278	-11900
n-Octane	1.944	21.14	287	-3670
p-Xylene	2.274	28.01	289	-2200

Table 3.1. Physical parameters for solvents characterized by the "ping-pong" technique. Physical constants at 293K are taken from Lide.[13] Theoretical evaporation parameters are calculated from equations (3.15)-(3.17).

3.7. Conclusions

The ping pong experiment presents a unique way of determining the evaporation and Rayleigh discharge dynamics of micron-sized droplets. Mobility measurements are performed in a mild, uniform, linear, switched DC electric field as opposed to the alternating AC fields employed in an electrodynamic balance experiments. In the ping-pong experiment, the field is repeatedly reversed following characterization of diameter, size, and charge by a phase Doppler anemometer. Repeated PDA characterizations create a history of the droplet in which Rayleigh discharge events are observed.

Modeling droplet behavior shows that larger 50 μm droplets are not well characterized by our ping-pong experiment because they do not reach equilibrium before they are analyzed by the PDA and therefore are not subject to the force-balance equation employed to determine charge. Smaller droplets do reach their equilibrium velocity and are accurately characterized by the PDA and the force-balance equations.

3.8. References

(1) Rayleigh, L. *Philos. Mag.* **1882**, *14*, 184.

(2) Feng, X.; Bogan, M. J.; Agnes, G. R. *Anal. Chem.* **2001**, *73*, 4499.

(3) Duft, D.; Lebius, H.; Huber, B. A.; Guet, C.; Leisner, T. *Phys. Rev. Lett.* **2002**, *89*, art. no. 084503.

(4) Duft, D.; Atchtzehn, T.; Muller, R.; Huber, B. A.; Leisner, T. *Nature* **2003**, *421*, 6919.

(5) Smith, J. N. Fundamental Studies of Droplet Evaporation and Discharge Dynamics in Electrospray Ionization, California Institute of Technology, 2000.

(6) Smith, J. N.; Flagan, R. C.; Beauchamp, J. L. *J. Phys. Chem. A* **2002**, *106*, 9957.

(7) Grimm, R. L.; Beauchamp, J. L. *Anal. Chem.* **2002**, *74*, 6291.

(8) Seinfeld, J. H.; Pandis, S. N. *Atmospheric chemistry and physics*; Wiley-Interscience: New York, 1998.

(9) Gerald, C. F.; Wheatley, P. O. *Applied numerical analysis*, 5th ed.; Addison-Wesley: Reading, MA, 1994.

(10) Hinds, W. C. *Aerosol Technology: Properties, Behaivor, and Measurement of Airborne Particles*, 2nd ed.; John Wiley & Sons, Inc.: New York, 1999.

(11) Yaws, C. L. *Chemical Properties Handbook: Physical, Thermodynamic, Environmental, Transport, Safety, And Health Related Properties for Organic and Inorganic Chemicals*; McGraw-Hill: New York, 1999.

(12) Vargaftik, N. B.; Vinogradov, Y. K.; Yargin, V. S. *Handbook of Physical Properties of Liquids and Gases: Pure Substances and Mixtures*, 3rd ed.; Begell House, Inc., 1996.

(13) *CRC Handbook of Chemistry and Physics*; 76th ed.; Lide, D. R., Ed.; CRC Press: Boca Raton, FL, 1995.